Study of X-ray generation by Laser Compton scattering

2002

Masaru Kimura

Contents

1 Introduction

1.1 Experimental background

Studies on Compton scattering of an electron and a laser has recently received much attention. It can generate a photon with high directivity and very wide energy from keV to hundred of GeV by choosing energy of the electron and the wavelength of the laser. This method is that the necessary energy to electron for generation of these photons can be lower than the usual means such as Synchrotron radiation. In the meaning of the X-ray generation, it implies that the generation of the X-ray in smaller accelerator facilities than an usual one is possible. And, in the meaning of super-high energy photon generation toward the atomic nucleus and elementary particle experiment with the photon, we have thought that Laser Compton scattering is the only way to do it.

1.2 Motivation to Laser Compton scattering experiment

In the above meanings, the photon generation by Laser Compton scattering is very interesting field. Based on these characters, we decided to study about X-ray generation by Laser Compton scattering at the electron ring, REFER (Relativistic Electron Facility for Education and Research), in Hiroshima University Venture Business Laboratory (Hi-VBL). When a laser pulse, the wavelength is 532nm, is irradiated to 150MeV electron beam provided by REFER, the X-ray of the maximum 800keV is generated.

This experiment is placed as the establishment of the generation of a high intensity X-ray by Laser Compton scattering and the fundamental study for the development of a new X-ray source by this means. In the future, this is placed as the fundamental development toward photon-photon collider[1].

1.3 Laser Compton scattering experiment at REFER in Hi-VBL

We performed to Laser Compton scattering at REFER in Hi-VBL. As a result, we constructed the experimental system for observing the scattered photons and actually observed scattered photons.

In this thesis, we will show the theoretical description of Laser Compton scattering (Chapter 2), the experimental setup and procedure (Chapter 3, 4), the experimental results (Chapter 5) and the numerical calculation of number of scattered photons and the simulation of energy spectrum for comparison with experimental results (Chapter 6, 7).

2 Theoretical description of Laser Compton scattering

2.1 Kinematics

In this section, we will show kinematics of Laser Compton scattering, a scattering process between an accelerated electron and a laser. Firstly, we will show kinematics of a scattering process of a rest electron and a photon which is the basis of Compton scattering. Secondly, we will show kinematics of a scattering process of 150MeV and a laser, our experimental situation.

2.1.1 Scattering of a photon and a electron at rest

As this process is an elastic collision, it is shown by the laws of conservation of energy and momentum as

$$E_1 + mc^2 = E_2 + mc^2\gamma, \tag{2.1}$$

$$\frac{E_1}{c} = \frac{E_2}{c}\cos\theta + mc\beta\gamma\cos\phi, \tag{2.2}$$

$$0 = \frac{E_2}{c}\sin\theta - mc\beta\gamma\sin\phi, \tag{2.3}$$

where E_1 is energy of the incident photon, E_2 is energy of the scattered photon, mc^2 is energy of electron at rest, $mc^2\gamma$ is energy of the scattered electron, γ is Lorentz factor, β is the velocity of the electron, θ is the scattering angle of photon, ϕ is the scattering angle of electron, m is the mass of the electron at rest and c is light velocity, respectively (Fig.2.1). From these equations, we obtain E_2 as

$$E_2 = \frac{mc^2 E_1}{mc^2 + E_1(1-\cos\theta)}. \tag{2.4}$$

From this equation, we find that energy of the scattered photon is uniquely determined by the scattering angle of it.

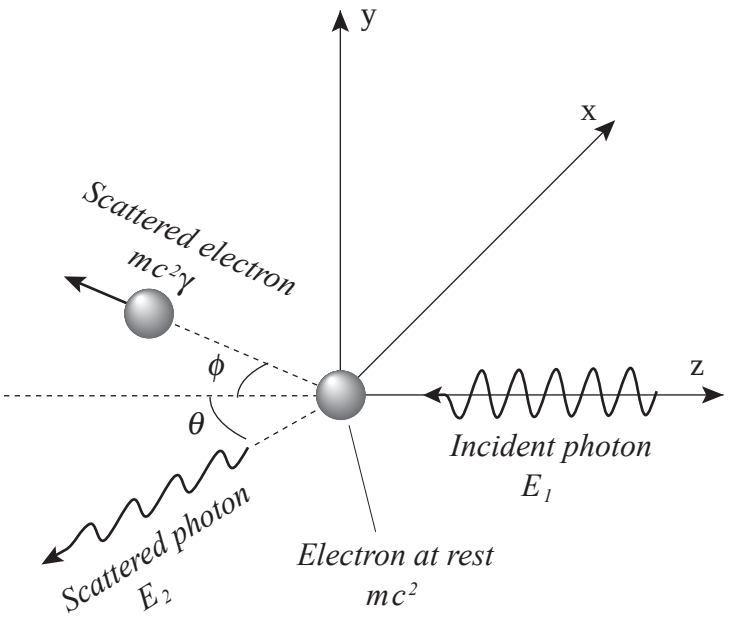

Figure 2.1: Scattering of a photon and an electron at rest.

2.1.2 Scattering of a photon and a 150MeV electron

This process is also shown by above two lows of conservation as

$$E_i + mc^2\gamma_i = E_s + mc^2\gamma_s, \tag{2.5}$$

$$\frac{E_i}{c} - mc\beta_i\gamma_i = \frac{E_s}{c}\cos\theta' + mc\beta_s\gamma_s\cos\phi', \tag{2.6}$$

$$0 = \frac{E_s}{c}\sin\theta' - mc\beta_s\gamma_s\sin\phi', \tag{2.7}$$

where E_i is energy of the incident photon, E_s is energy of the scattered photon, $mc^2\gamma_i$ is energy of the incident electron, $mc^2\gamma_s$ is energy of scattered electron, both of γ_i (γ_s) and β_i (β_s) are the factors of the Lorentz transformation, θ' is the scattering angle of photon and ϕ' is the scattering angle of electron, respectively (Fig.2.2). From these equations, we obtain E_s as

$$E_s = \frac{mc^2\gamma_i E_i(1+\beta_i)}{mc^2\gamma_i(1+\beta_i\cos\theta') + E_i(1-\cos\theta')}. \tag{2.8}$$

From this equation, we find the maximum and minimum energy of the scattered photon. When $\theta' = \pi$ [rad], the former is about 800keV, and when $\theta' = 0$[rad], the latter is 2.33eV.

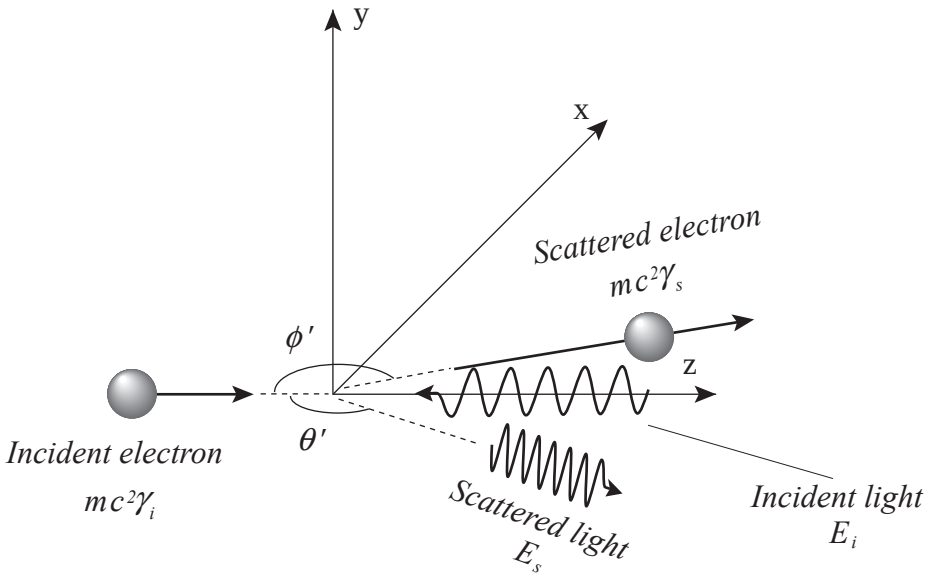

Figure 2.2: Scattering of a photon and a 150MeV electron.

2.2 Cross section in photon – 150MeV electron scattering

2.2.1 Differential cross section

The differential cross section of Compton scattering is given by the Klein-Nishina formula[2]:

$$\frac{d\sigma}{d\Omega} = \frac{r_e^{\,2}}{2}\left(\frac{E_2}{E_1}\right)^2\left(\frac{E_1}{E_2}+\frac{E_2}{E_1}-\sin^2\theta\right). \tag{2.9}$$

Where σ is the cross section, Ω is the solid angle of the scattered photon at the free electron scattering process and r_e is the classical electron radius ($e^2/4\pi\varepsilon_0 mc^2$) respectively. In fact, however, since we will observe 150MeV electron scattering, we must convert Eq.2.9 to the appropriate forms. Then we need $d\sigma/dE_s$ and $d\sigma/d\Omega'$, and these are written as

$$\frac{d\sigma}{dE_s} = \frac{d\sigma}{d\Omega}\frac{d\Omega}{dE_s} = \frac{d\sigma}{d\Omega}(-2\pi)\frac{d\cos\theta}{dE_s}, \tag{2.10}$$

$$\frac{d\sigma}{d\Omega'} = \frac{d\sigma}{dE_s}\frac{dE_s}{d\Omega'} = \frac{d\sigma}{dE_s}\frac{dE_s}{(-2\pi)d\cos\theta'}, \tag{2.11}$$

where Ω' is the solid angle of the scattered photon at the 150MeV electron scattering process. From the Lorentz transformation of energy of the scattered photon, E_s is obtained as

$$E_s = \gamma_i E_2 - \beta_i \gamma_i E_2 \cos\theta = \gamma_i E_2 (1 - \beta_i \cos\theta). \tag{2.12}$$

Then, from Eq.2.4 and Eq.2.12, E_s is written as

$$\begin{aligned} E_s &= \gamma_i (1 - \beta_i \cos\theta) E_2 \\ &= \gamma_i (1 - \beta_i \cos\theta) \frac{mc^2 E_1}{mc^2 + E_1 (1 - \cos\theta)}. \end{aligned} \tag{2.13}$$

Then, $d\cos\theta/dE_s$ is obtained as

$$\frac{d\cos\theta}{dE_s} = \frac{mc^2 + E_1}{E_1 (E_s - mc^2 \beta_i \gamma_i)} - \frac{E_1 E_s (mc^2 + E_1)}{\{E_1 (E_s - mc^2 \beta_i \gamma_i)\}^2} + \frac{mc^2 \gamma_i}{(E_s - mc^2 \beta_i \gamma_i)^2}. \tag{2.14}$$

Therefore, $d\sigma/dE_s$ is obtained from Eq.2.9, Eq.2.10 and Eq.2.14. From Eq.2.1.8, $dE_s/d\cos\theta$' is written as

$$\frac{dE_s}{d\cos\theta'} = -\frac{E_i mc^2 \gamma_i (1 + \beta_i)(mc^2 \beta_i \gamma_i - E_i)}{\{mc^2 \gamma_i + E_i + (mc^2 \beta_i \gamma_i - E_i)\cos\theta'\}^2}. \tag{2.15}$$

Therefore, $d\sigma/d\Omega$' is obtained from Eq.2.9, Eq.2.10, Eq.2.11 and Eq.2.15. Thus, we obtain the theoretical energy spectrum and angle distribution of the scattered photons. These are shown in Fig.2.3 and Fig.2.4. These figures show that there are the scattering energy peak at about 800keV and the scattering angle peak at π rad.

2.2.2 Total cross section

The total cross section of the Compton scattering is written as

$$\sigma = \int \frac{d\sigma}{d\Omega} d\Omega. \tag{2.16}$$

The integration of Eq.2.16 over the whole space is as follows.

$$\sigma \cong 6.65 \times 10^{-25} [cm^2]. \tag{2.17}$$

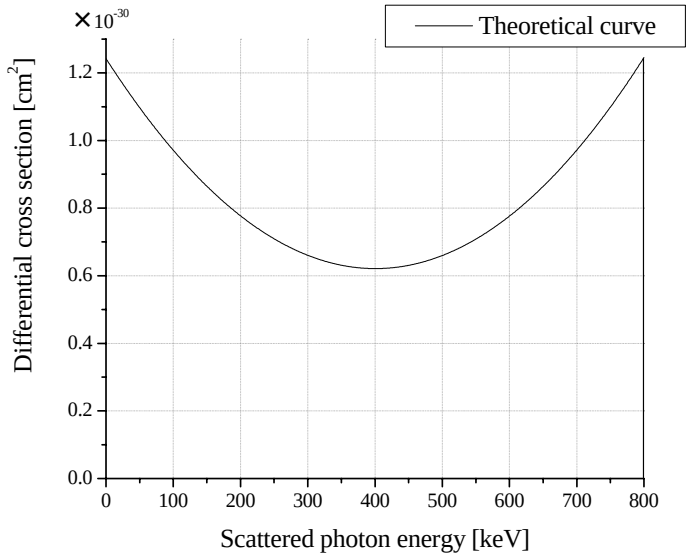

Fig.2.3: Theoretical energy spectrum of scattered photons at the 150MeV electron scattering process.

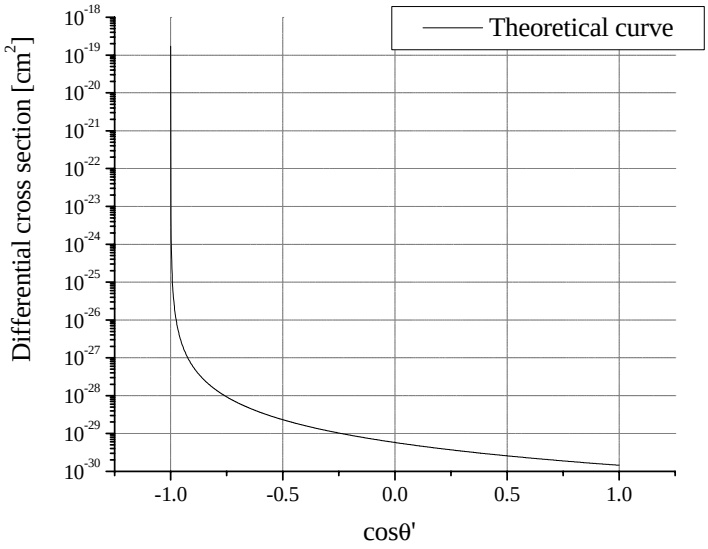

Fig.2.4: Theoretical angle distribution of scattered photons at the 150 MeV electron scattering process.

3 Experimental setup

3.1 Overview of the experimental setup

We performed to Laser Compton scattering at REFER in Hi-VBL. The overview of the experimental setup is shown in Fig.3.1. It consists of the electron, laser, optics and detection system. The electron beams are provided by the microtron of 150MeV beam energy, and they are injected into REFER through the beam transport. Laser pulses are provided by Q-Switched Nd-YAG laser, and they are injected into REFER through the optics system consists of mirrors and a condensing lens through the laser port. The scattered photons generated by the collisions between the electron beams and laser pulses are observed by NaI detector.

3.2 Electron beam

As the electron acceleration and injection device to REFER, we have used the microtron which is for Hiroshima University Synchrotron Orbit Radiation (HiSOR), the electron storage ring in Hiroshima Synchrotron Radiation Center (HSRC). The main specifications are shown in Table.3.1. These are maximum specifications. In our actual operation, however, the pulse length, maximum current and repetition were 0.2μs, 2mA and 10Hz, respectively.

The electrons injected to REFER have lost their energy with circling and disappears at last. It is shown in Fig.3.2, measured by using the current monitor (CT). In this figure, we found that the electron beam current decreased rapidly after about 1ms from injecting the electron beam, then decreased slowly for about 1.5ms, and at last disappeared after about 3ms. The vertical beam diameter is also about 20mm[3].

3.3 Laser beam line

The laser beam line consists of Q-Switched Nd-YAG laser and the optics system as shown in Fig.3.3. Q-Switched Nd-YAG laser, called SAGA, is manufactured by the BM industries, Inc. The main specifications are shown in Table.3.2. SAGA is also operational as the external trigger mode, and we externally triggered flashlamp of the laser. The optics system consists of three dielectric mirrors and a condensing lens. The reflection rate of the dielectric mirrors is about 100% to 532nm wavelength. The focal length and the diameter of the condensing lens are 2000mm and 100mm respectively, and it has the anti-reflection coat, its permeation rate is about 99.4 % to 532nm wavelength. The laser pulses emitted from the Nd-YAG laser are led to the front of the laser port about 3m ahead by three mirrors, and irradiate the electron beams about 2m ahead through the condensing lens. Also, we had switched the laser injection to the laser port by remote control of the mirror on the motorized stage at the laser upstream. This is the system of using CAMAC.

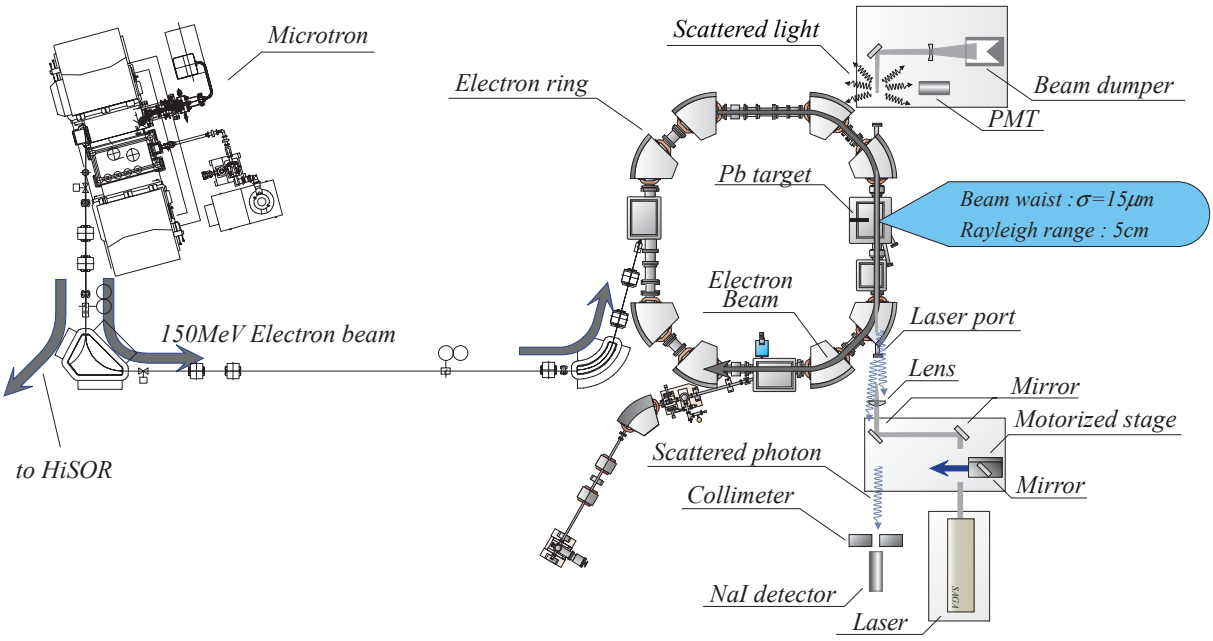

Fig.3.1: Overview of the experimental setup.

Table.3.1: Main specification of microtron.

item	**value**
Electron energy	150 MeV
Peak current	10 mA
Pulse length	2 μs
Emittance	π mm･mrad
Repetition rate	100Hz

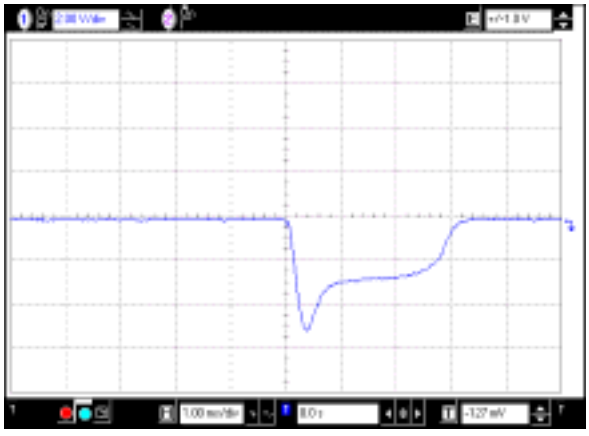

Fig.3.2: Electron beam current. One-divisions of the horizontal and vertical axes are 1ms and 2V respectively. 1V corresponds to the electron beam current of 2mA[4].

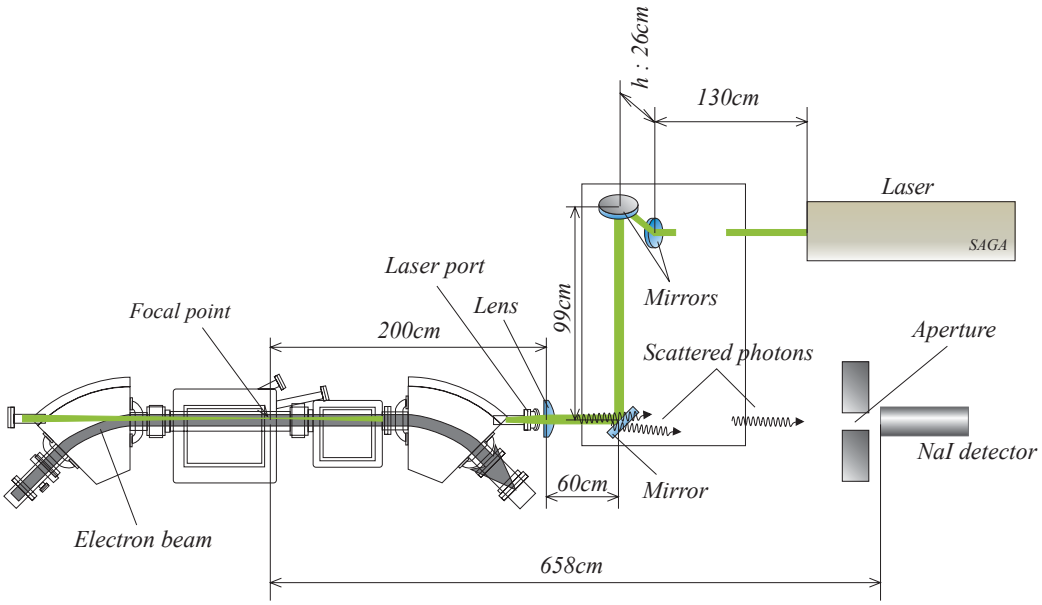

Fig.3.3: Laser beam line. This consists of the Q-Switched Nd-YAG laser and the optics system. After the laser pulses emitted from Nd-YAG laser are led to the front of the lens about 3m ahead by three mirrors, they irradiate the electron beams about 2m ahead through the condensing lens.

Table.3.2: Main specification of Q-Switched Nd-YAG laser.

item	**value**
Repetition rate	10 Hz
Wavelength	532 nm
Energy per pulse	600 mJ
Pulse width	5-7 ns
Beam diameter	9mm
Beam divergence	0.5 mrad
Jitter unseeded	±0.5
seeded	±2
Energy stability (rms)	1.2%
Polarization	Horizontal

3.4 Detection system for the scattered photons

Detection system is shown in Fig.3.4. We selected the NaI detector as the photon detector. The crystal of NaI has enough thickness, 2 inch, to detect 800keV X-ray. Lead and concrete blocks surround the detector to protect it from the background of the electron beam. Lead blocks of the downward, upward and laser port direction are the thicknesses of 3cm, 5cm and 50cm, respectively. The concrete block of the downward direction is thickness of 20cm. there is also the polyethylene block, the thickness of 5cm, on the top of the detection system. It is effective

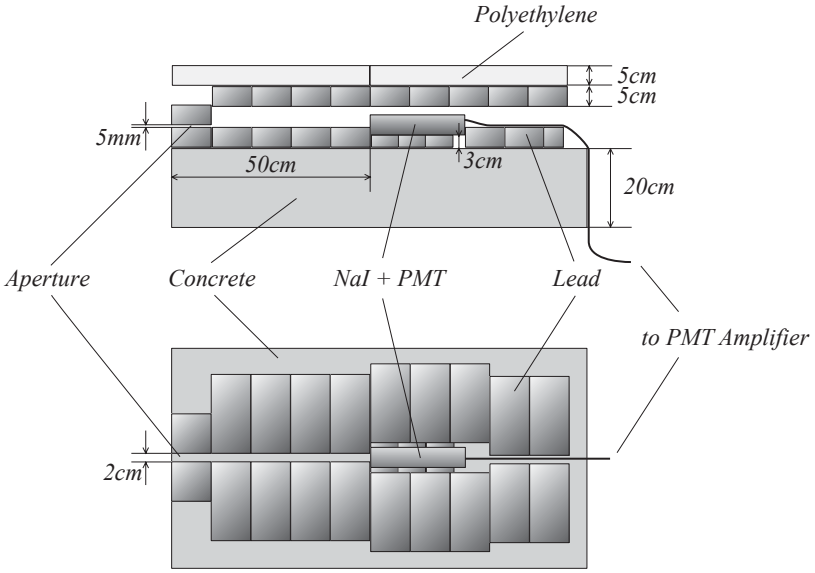

Fig.3.4: Detection system for the scattered photons. Upper figure and lower one are side view and top view of it respectively.

to protect the detector from the low energy neutrons. There is the aperture in front of the detection system, the horizontal and vertical directions are lengths of 2cm and 5mm respectively.

3.5 Data acquisition system

The overview of data acquisition system (DAQ system) is shown in Fig.3.5. The analog signals obtained from NaI detector are and photo-multiplier-tube (PMT) are amplified through the PMT amplifier near these in the REFER room, and then transmitted to the REFER control room. After the signals go through many NIM modules, they are digitized through CAMAC module so that these data are input into the PC-1 there. Motorized stages are also controlled by CAMAC module and driven by another PC-2. These PCs are connected to a network each other, and the PC-1 can perform the remote control of the PC-2. After all, This DAQ system can be controlled by only the PC-1 in REFER room without entering the REFER room even during the operation time of microtron and REFER.

Timing chart until a laser pulse is externally emitted is shown in Fig.3.6. The signal synchronized with microtron timing but delayed is applied to the External Trigger Lamp Input of the laser system. It is possible to adjust this delay to 300ns ~ 1.2ms. After a delay of 180μs, the External Trigger Q-Switch Output is provided from the laser system, and after a delay of 600ns, a laser pulse is emitted so that PMT Output at Laser Downstream is provided because of a laser pulse scattered by atmosphere.

Flowchart of the basic data taking system is schematically shown in Fig.3.7. The External Trigger Q-Switch Output from the laser system and PMT Output at Laser Downstream provide

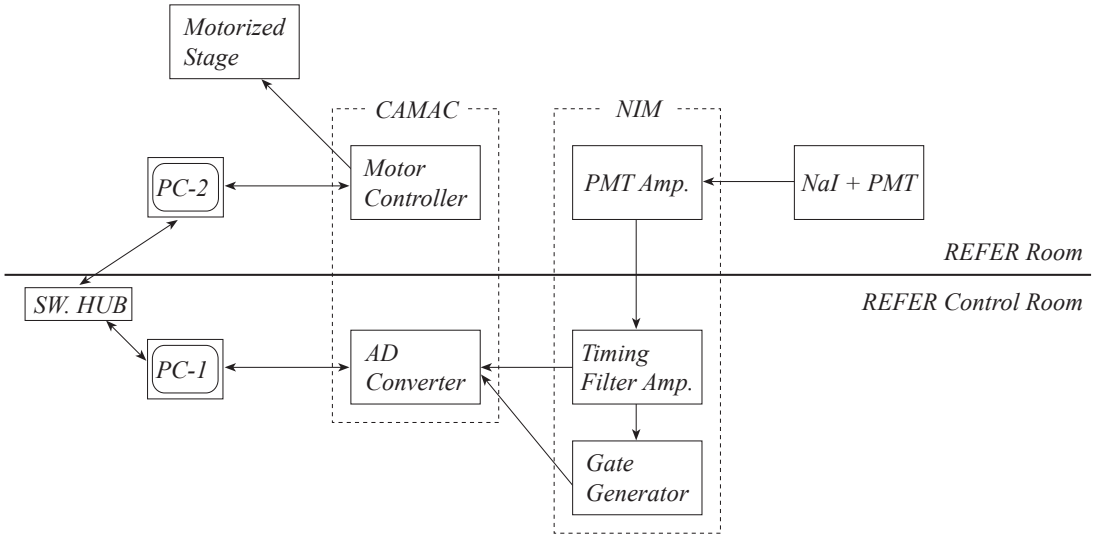

Fig.3.5: Overview of data acquisition system.

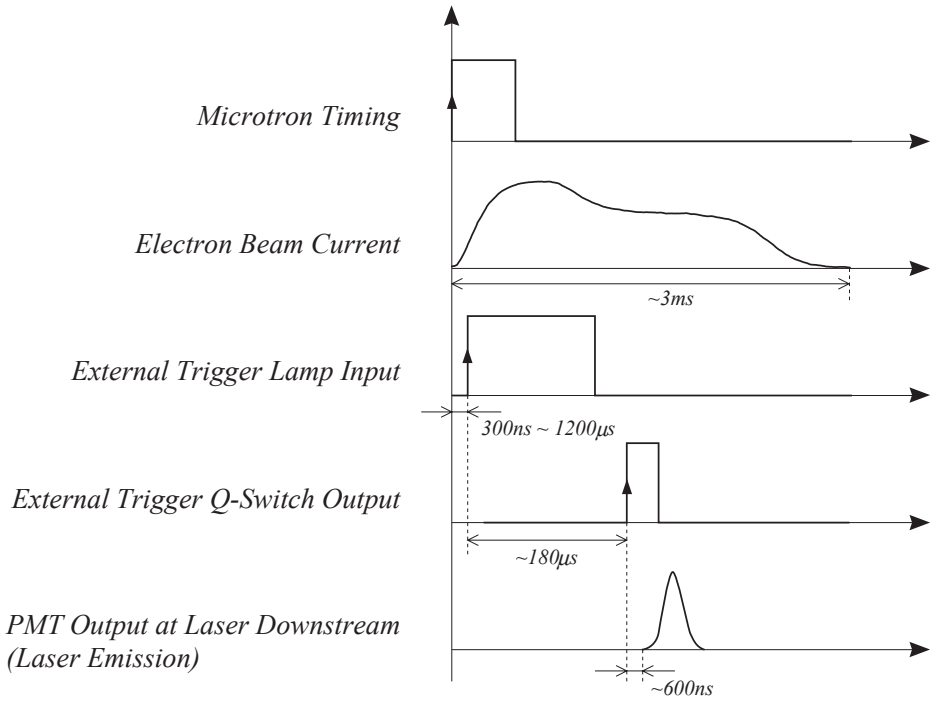

Fig.3.6: Timing chart until a laser is externally fired.

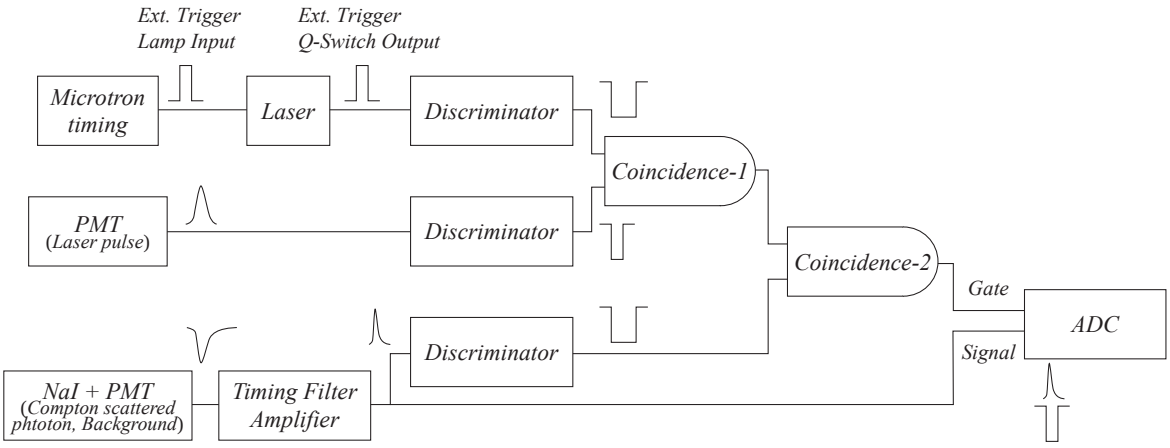

Fig.3.7: Flowchart of daata taking system. The basic modules are only shown. Actually, since the rising of output signals from Laser, PMT and NaI + PMT shifted each other, we had to use many delay modules everywhere. The pulse duration of these input signals into Coincidence-1 are 200ns and 20ns respectively. With regard to Coincidence-2, the pulse duration of the output signals from Coincidence-1 and NaI + PMT are 20ns and 200ns respectively. Except for ADC CAMAC module, Timing Filter Amplifier, Discriminator and Coincidence are NIM modules.

trigger signals for laser-electron scattering into Coincidence-1. Then, Coincidence-1 and output from NaI detector and PMT differentiated through Timing Filter Amplifier (TFA) are input into Coincidence-2. Finally, Coincidence-2 provides trigger (gate) signals for the analog output signals, have the height information, from TFA into peak-hold AD-Converter (ph-ADC). The ph-ADC digitizes the pulse height of the analog input signals with 12bit.

In order to take two kinds of data, the information of energy of scattered photons and background, we had to switch the laser injection to the laser port by remote control of the mirror on the motorized stage at the laser upstream. If we want to take data of background, we make it move on the laser beam line and reflect laser pulse not to irradiate the electron beam, and then we input only the external trigger Q-switch outputs into Coincidence-1. With regard to data of scattered photons, we make it remove from the laser beam line, and then we input the external trigger Q-switch outputs and PMT outputs into Coincidence-1.

3.6 Laser multi pass system

We show another optics system, the laser multi pass system, in Fig.3.8. This system consists of four mirrors and tow lenses, and we can recycle the laser pulses by this system so that we can expect 2~3 times increase in the number of scattered photons as comparison with our usual single pass system. These mirrors are the same as the above-mentioned ones. Two lenses are the same as each other, these focal length and the diameter are 2000mm and 100mm respectively. We aligned these lenses as both ones had the same focal point and these mirrors as the laser pulses were injected to all mirrors at the incident angles of 45 degrees.

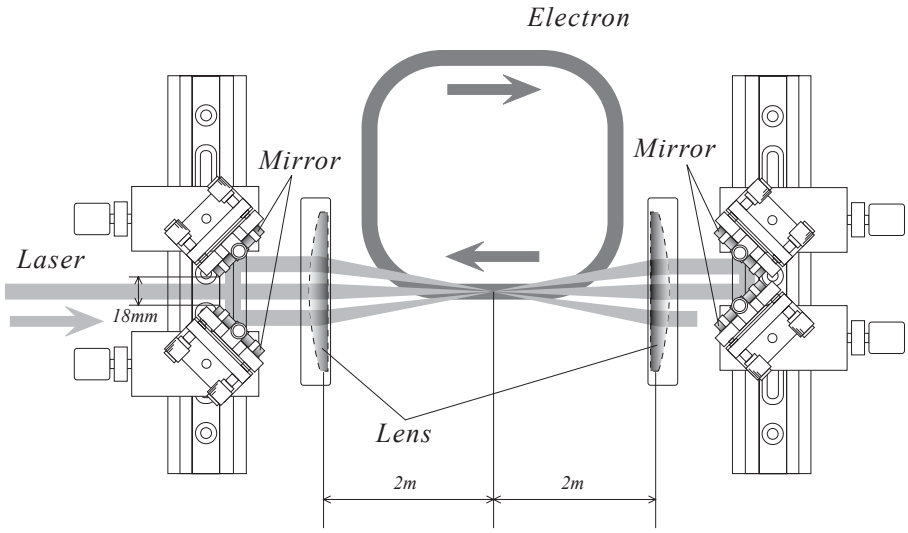

Fig.3.8: Laser multi pass system.

4 Experimental procedure

4.1 Time dependence of the electron beam position

In section 3.2, we explained the time dependence of the electron beam current. On the other hand, we will explain the time dependence of the electron beam position in this section.

The time dependence of the electron beam position is shown in Fig.4.1[3]. This figure was obtained by the SR monitor. In this figure, we found that the horizontal position of electron beam changed with time passing. The electron beam moved to the inside of the beam pipe about 15mm from injecting it. Therefore, we had to adjust the laser injection position and the laser injection timing to electron beam respectively.

4.2 Search for the laser injection position and the detector position

The requirement for searching the better laser injection position depends on whether this position is the one scattered photons come to the detector more efficiently. The searching system is shown in Fig.4.2. There is the internal lead target, 1.3mm of thickness and 3mm of width, inside REFER as shown in Fig.3.1 and we can put it in and out toward the electron beam. As shown in Fig.4.2, we make the target interact with the electron beam at several positions so that the bremsstrahlung photons corresponding to the positions of target are generated along the proceeding direction of the electron beams. If we make the laser irradiate the electron beam corresponding to a position of the target, the scattered photons will be generated to the same direction as the bremsstrahlung photons. Then, we counted the numbers of bremsstrahlung photons at the downstream area by scanning with the two plastic scintillators, the overlap of them was 5mm. As a result, we obtained the profiles of the bremsstrahlung photons in Fig.4.3 so that we determined the laser injection position and the detector position from the target position and the profile of bremsstrahlung photons respectively.

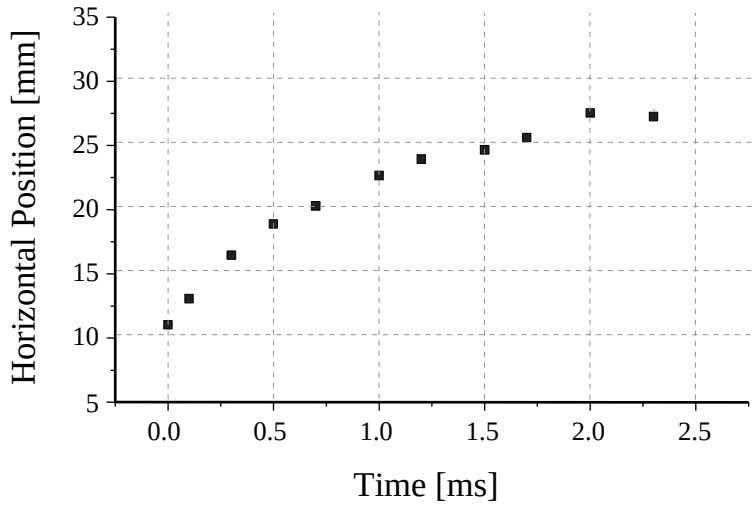

Fig.4.1: Time dependence of the horizontal position of the electron beam. 17.5 mm of horizontal position corresponds to the center of the beam pipe, and the large value of the horizontal position corresponds to the inside of the beam pipe.

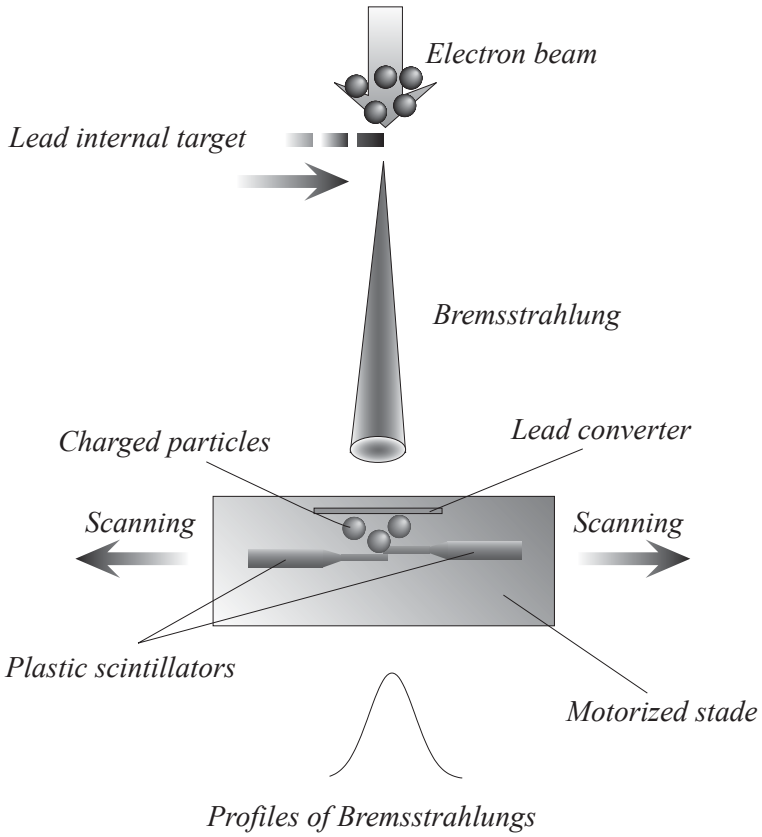

Fig.4.2: Searching system for the laser injection position and the detector position.

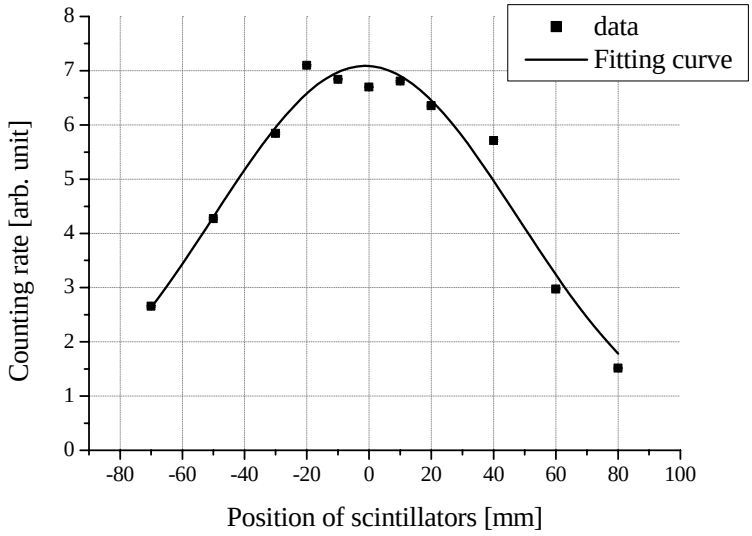

Fig.4.3: Profile of bremsstrahlung.

5 Experimental results

5.1 Optimization of the laser injection timing

Though the laser injection timing for efficient collisions between electron beams and laser pulses is uniquely determined by the position of the electron beam as shown in Fig.4.1, we must optimize it because the pulse width of the laser, about 6ns, is shorter than the time interval we measured the position of the electron beam. We used the timing signal from microtron as the laser external trigger as shown in Fig.3.6, and we scanned the yield of scattered photons with NaI detector by changing the laser injection timing. The results are shown in Fig.5.1. In this figure, the counting rate of only Compton scattered photons at 800μs is 0.224±0.001 photons per laser pulse.

5.2 Results

The experimental result is shown in Fig.5.2. In this figure, gray spectrum represents the addition of Compton scattering and background events and black one represents background events only. The threshold of energy is about 200keV.

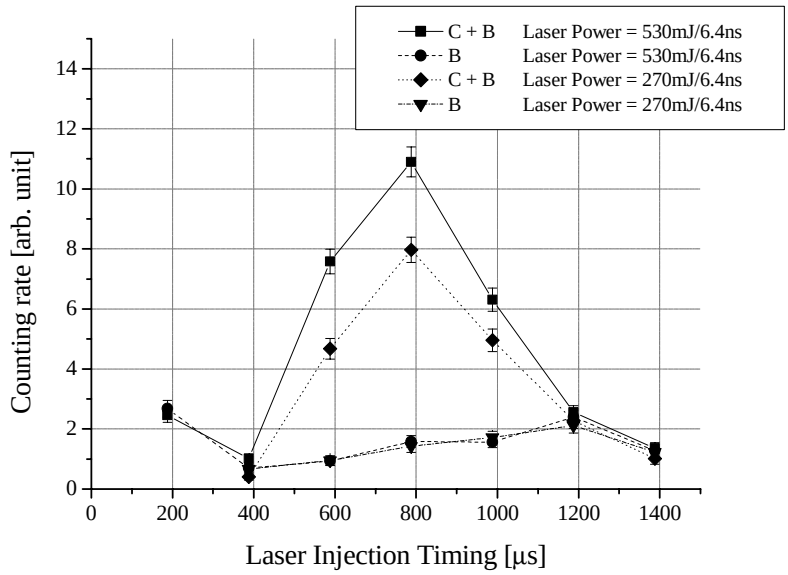

Fig.5.1: Dependence on the laser injection timing of the counting rates of NaI detector. In this figure, “C” and “B” represent data of Compton scattered photons and Background respectively.

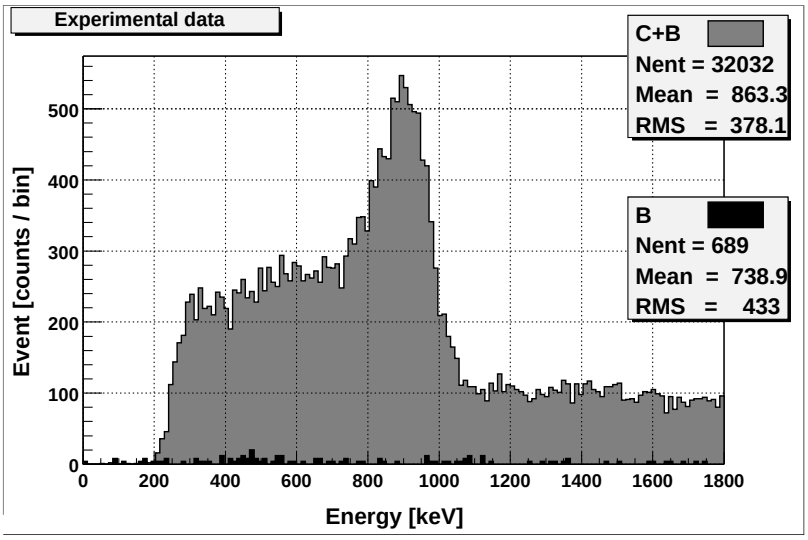

Fig.5.2: Spectra of Compton scattered photons and background. C and B represent Spectra of Compton scattered photons and background respectively.

6 Numerical calculation of number of scattered photons

In order to confirm whether the experimental data agreed with the theoretical value, we calculated the number of the scattered photons which come to the detector under the same condition as the experiment.

6.1 Process to calculating the number of the scattered photons

The number of scattered photons, $dN_{compton}$, at the time, dt, in the volume, dV, is written as[5]

$$dN_{compton} = 2c\sigma_c(z)n_p(r,z,t)n_e(r)dtdV, \tag{6.1}$$

where $\sigma_c(z)$ is the cross section, $n_p(z,r,t)$ is the number density of the pulse laser and $n_e(r)$ is the number density of the electron beam, respectively. The total number of the scattered photons, $N_{compton}$, is written as

$$\begin{aligned} N_{compton} &= \int_{V,t} dNdVdt \\ &= \int_{V,t} 2c\sigma_c(z)n_p(r,z,t)n_e(r)dVdt. \end{aligned} \tag{6.2}$$

Therefore, we can calculate it by finding $\sigma_c(z)$, $n_p(z,r,t)$ and $n_e(r)$.

6.2 Number density of the electron beam

The number density of the electron beam, n_e, is written as

$$n_e = N_e \times D_e, \tag{6.3}$$

where N_e is the number of electrons per unit length and D_e is the distribution function of the electron beam in the x and y direction respectively. The former is written as

$$N_e = \frac{V}{0.5} \times \frac{1}{ce} \times 10^{-3} \ \ [electorns/m], \tag{6.4}$$

where V is the reading value of the voltage on the beam current monitor[4] (Fig.4.1) and e is the electric charge. If the latter is a gauss distribution, it is written as

$$D_e = \frac{1}{2\pi\sigma_{er}^2}\exp\left(-\frac{r^2}{2\sigma_{er}^2}\right)\ [m^{-2}], \tag{6.5}$$

where σ_{er} is the dispersion of the electron beam in the radius direction as shown in Fig.6.1. From these equations, we obtain the number density of the electron beam.

6.3 Number density of the laser pulse

The number density of the laser pulse, n_p, is written as

$$n_p = N_p \times D_p, \tag{6.6}$$

where N_p is the number of photons per unit pulse and D_p is the distribution function of the laser pulse in the x, y and z direction respectively. The former is written as

$$N_p = P \div \frac{hc}{\lambda}\ [photons/pulse], \tag{6.7}$$

where P is the power of the laser pulse, h is Plank constant, c is light velocity and λ is the wavelength of the laser. If the latter is a gauss distribution, it is written as

$$D_p = \frac{1}{(2\pi)^{3/2}\sigma_{pr}^2\sigma_{pz}}\exp\left\{-\left(\frac{r^2}{2\sigma_{pr}^2}+\frac{(z-ct)^2}{2\sigma_{pz}^2}\right)\right\}\ [m^{-3}], \tag{6.8}$$

where σ_{pr} and σ_{pz} are the dispersions of the laser pulse in the radius direction and in the proceeding direction as shown in Fig.6.2 respectively, and the former is written as[6]

$$\sigma_{pr} = \sigma_0\left(1+\left(\frac{\lambda z}{4\pi\sigma_0^2}\right)^2\right)^{\frac{1}{2}}, \tag{6.9}$$

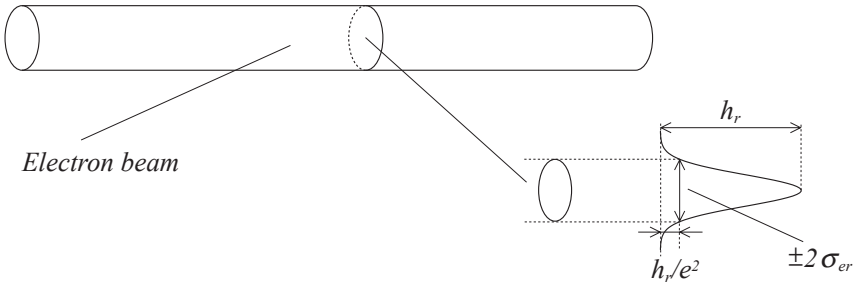

Fig.6.1: Intensity distribution of electron beam.

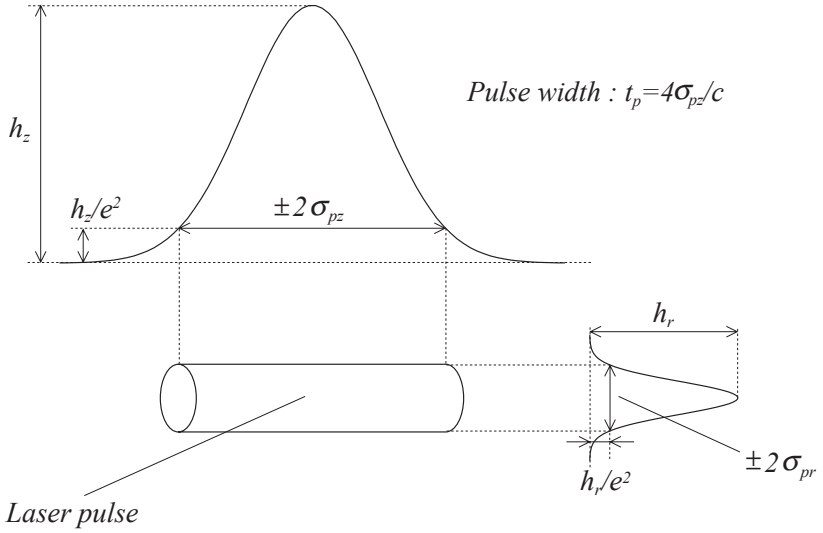

Fig.6.2: Intensity distribution of laser pulse.

where σ_0 is the dispersion of the laser pulse at the beam waist in the radius direction. It is shown in Fig.6.3. From these equations, we obtain the number density of the laser pulse, too.

6.4 Laser – electron interaction region

The interaction situation of the laser pulse and the electron beam is shown in Fig.6.4. l is the interaction length and t_p is the pulse width of laser pulse respectively. In this case, the interaction length in z direction is l of the overlap region of the electron beam and the laser pulse. Since the center of l is $z = 0$, the integration region of z direction is $-l/2 \sim l/2$. Since interaction begins at the time the end of laser pulse enters into the overlap region, the integration time t is $-(l/2c + t_p/2) \sim (l/2c + t_p/2)$ if the center of laser pulse pass the center of the overlap region at $t = 0$.

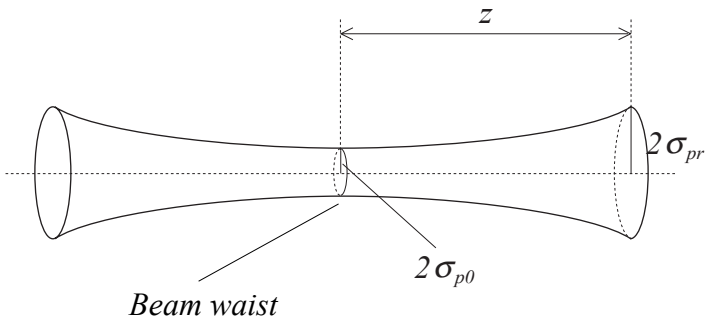

Fig.6.3: Dependence on *z* of dispersion of laser pulse

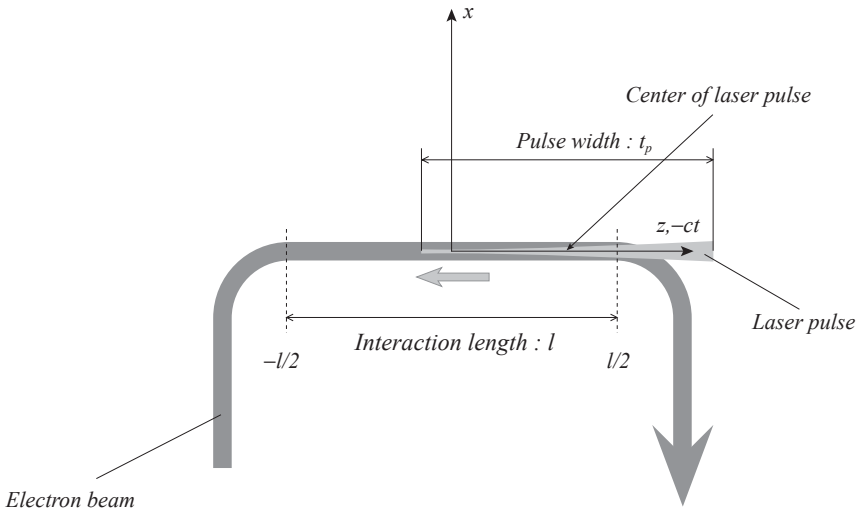

Fig.6.4: Interaction situation of laser pulse and electron beam.

6.5 Detection region of scattered photons

For reasons of the solid angle of scattered photon and the detection system for scattered photons as shown in Fig.3.4, there is the limit to the detection region. In Fig.6.5, the interaction length of the electron beam and the laser pulse, from *A* to *B*, is 2m, the width of the aperture in front of NaI is 2cm and the distance from the center of interaction region to NaI is about 6.6m respectively. In this case, for example at the point A, the aperture of the detector is determined by the angle θ'_A, and then, the number of scattered photons arrive at the detector from the point A is calculated by the angle θ'_A as

$$\sigma'_c(z) = \int_{-1}^{\cos(\pi-\theta')} \frac{d\sigma_c}{d\cos\theta'} d\cos\theta', \qquad (6.10)$$

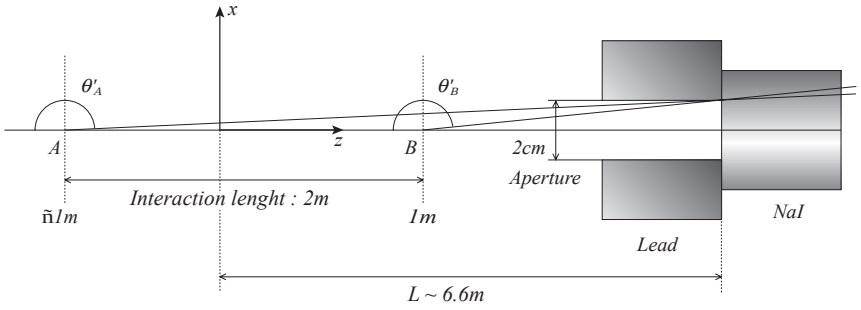

Fig.6.5: Detection region of scattered photons.

where θ' is the limited angle and $\sigma'_c(z)$ is the cross section from $\theta' = \theta'_A$ to π at z = –1. θ' is defined as

$$\theta' = \frac{10\times10^{-3}}{L-z}\ [rad], \tag{6.11}$$

where L is the distance from the center of interaction region to the detector. Then the total number of scattered photons arrive at the detector from all interaction points is calculated by integrating about the whole interaction rage, from $z = -1$ to 1.

6.6 Estimation of the number of the scattered photons

As stated above, we can calculate the total number of scattered photons arrive at the detector. The number is written as

$$\begin{aligned} N_{compton} &= 2c\int_{V,T}\sigma'_c(z)n_e(r)n_p(r,z,t)dVdt \\ &= 2c\int_{-l/2}^{l/2}\left\{\sigma'_c(z)\times 2\pi\int_0^{\infty}\left(n_e(r)\int_{-(l/2c+t_p/2)}^{l/2c+t_p/2}n_p(r,z,t)dt\right)rdr\right\}dz \end{aligned} \tag{6.12}$$

Then the total number of scattered photons arrive at the detector was obtained as

$$N_{compton} \sim 3.99 \text{ [photons/pulse]} \tag{6.13}$$

The parameters we used to calculate this value was as follows.

Table.6.1: Parameters of numerical calculation

Item	symbol	Value
Light velocity	c	299 792 458 m/s
Plank constant	h	$6.626\ 176\times10^{-34}$ J·s
Electron energy	$mc^2\gamma_i$	150 MeV
Electron rest mass	mc^2	0.511 003 4 MeV
Classical electron daius	r_e	2.817 938 0 fm
Electric charge	e	$1.602\ 189\ 2\times10^{-19}$ C
Electron diameter ($\pm2\sigma$)	$4\sigma_{er}$	19.16 mm
Electron beam current at CT monitor	V	225 mV
Laser wavelength	λ	532 nm
Laser power	P	445 mJ
Laser pulse width	t_p	6.4 ns
Laser diameter at beam waist ($\pm2\sigma$)	$4\sigma_{p0}$	63.1329 μm

7 Simulation

In order to analyze the energy spectrum, we simulated the responses of the detector by Geant4. This simulation program consists of the geometry of the detector, the interactions between the particles and the materials, the tracking of the particles, the responses of the detector and so on. Except for these, we had to prepare the event generator, the photon detection system and the energy resolution generator for the detector.

7.1 Event generation

The event generator provides energy, momentum of scattered photon (Gun) and a collision point. The distribution of energy is determined by Eq.2.10, which was led from the Klein-Nishina formula, and momentum is determined by energy and Eq.2.8. With regard to the collision point, the distribution of the electron-photon colliding points in the z direction is proportional to $1/\sigma_{pr}$, and in the r direction is proportional to $D_{er}(\boldsymbol{x})D_{pr}(\boldsymbol{x})$, where σ_{pr} is the dispersion of the laser pulse in the r direction, $\boldsymbol{x} = (x,y,z)$, $D_{er}(\boldsymbol{x})$ and $D_{pr}(\boldsymbol{x})$ are the distribution functions of the electron beam and the laser pulse in the r direction, respectively. For the interaction length of electron beam and the laser pulse, since $D_{pr}(\boldsymbol{x}) >> D_{er}(\boldsymbol{x})$, we considered $D_{er}(\boldsymbol{x})D_{pr}(\boldsymbol{x})$ as $D_{pr}(\boldsymbol{x})$ more simply.

7.2 Photon detection system

The photon detection system is shown in Fig.7.1. We considered NaI crystal as the cube with sides 2inch long. The distance from the center of the interaction region of the electron beam and the laser pulse to the NaI crystal is 658cm and the horizontal aperture in front of NaI crystal is 20mm. After event generator determines above three parameters, it is determined by the photon detection system whether Compton scattered photon comes into the NaI crystal. If the scattered photon interacted with the material, the total energy deposit of the scattered photon in the material will be obtained.

7.3 Energy resolution generator for the detector

We included the energy resolution generator for the detector in Geant4 source code. In this simulation, we used the energy resolution as σ_E/E, where σ_E is the dispersion of energy and it is shown in Fig.7.2. The fitting function is written as

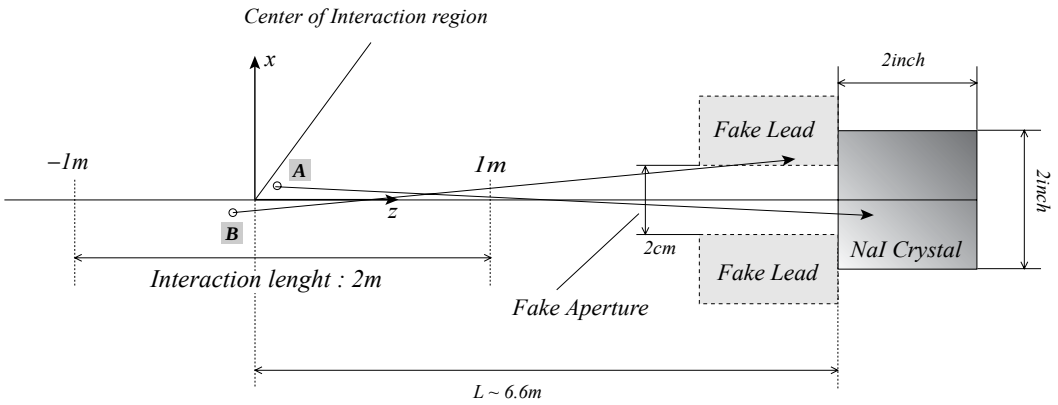

Fig.7.1: Photon detection system. This system has NaI Crystal for detecting a photon and a fake aperture constructed two fake leads for killing a photon. For example, one photon “A” comes into the detector without being killed by the fake leads, but another one “B” is killed by the fake one.

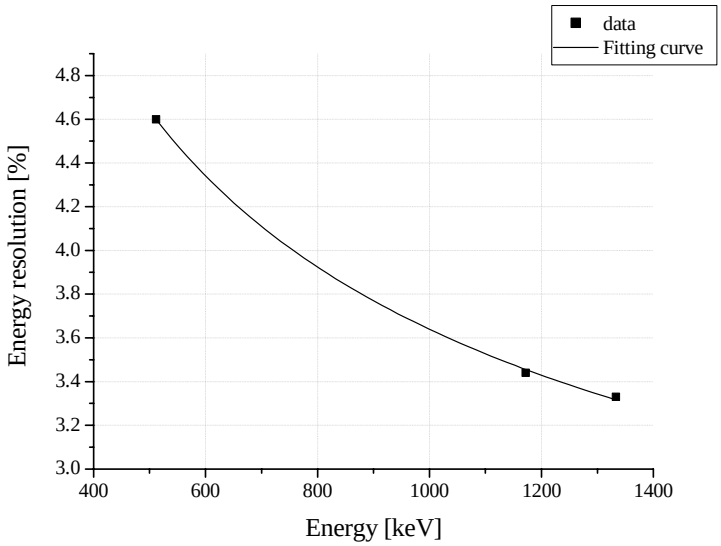

Fig.7.2: Energy resolution of NaI detector.

$$\frac{\sigma_E}{E} = a + \frac{b}{\sqrt{E}}, \tag{7.1}$$

where a and b are the fitting parameters. If the total energy deposit was obtained, the energy resolution generator for the detector will generate the energy resolution to it. Finally, output of the detector is determined by the Gaussian random number generator with the dispersion of energy.

The flowchart of the simulation code is shown in Fig.7.3.

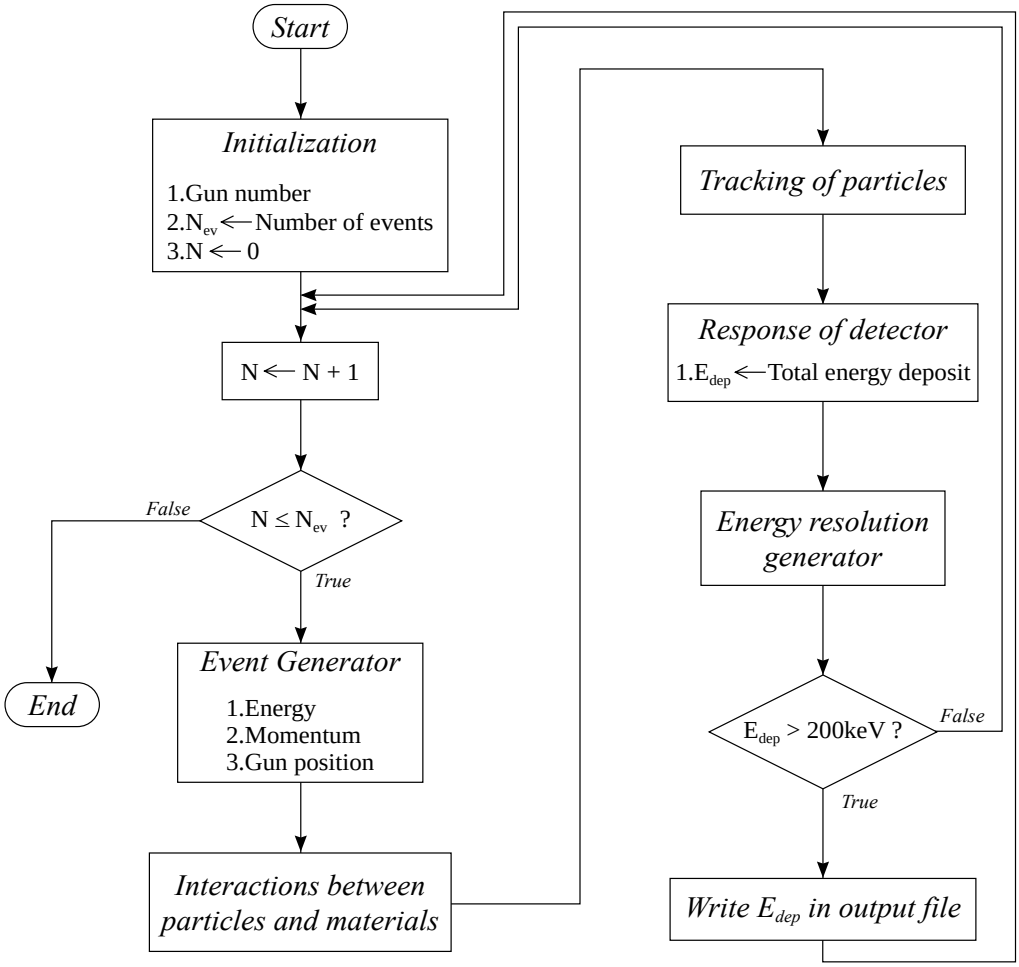

Fig.7.3: Flowchart of the simulation code.

8 Discussion

In Fig.5.1, there are enhancements at specific timing, and the signal intensity in NaI detector also has the dependence on the laser power. The former implies the generation of the scattered photons. However, the later shows the consistency with the theory, which we showed in Chapter 6. In other words, these results indicate the generation of the scattered photons. The former also implies the form of the electron beam. For taking the data for the energy spectrum, we optimized the laser injection timing to 800μs. The average number of scattered photons at this timing is also obtained as 0.224±0.001 [photons/pulse]. This value had a rough agreement with the calculating one (Eq.6.13) because this calculation is ideal in points of the electron-photon colliding point and timing, and the intensity distributions of electron beam and laser beam.

In Fig.5.2, there is the energy peak as shown in Fig.2.3, and the events of Compton scattered photons and background is clearly larger than the events of background only as mentioned above. However, there are the shift of the energy peak from about 800keV to higher energy region and the considerable events in the higher energy region over the peak.

The former is completely inconsistent with kinematics. Then, we have considered that it was caused by the condition during taking the data for the calibration of the detector because the electron beam is off when we took these data. There is a possibility that there is a noise effect, such as DC component, on the detector when the electron beam is on, and the calibration may be better under this condition. Actually, we show the spectra which the conditions are different in Fig.8.1. The spectra are the addition of Compton scattering and background events, but the conditions under which we took the data for the calibration of the detector were different each other. The gray spectrum and the white one were calibrated with the electron beam off and on, respectively. In this figure, we found that the energy peak of the later became lower than the former and less than 800keV. However, since the timing when we took these data for the calibration of the later to the electron beam current (Fig.3.2) was 4ms after the microtron timing and different from 800μs of the laser injection timing, this calibration is only reference. In this meaning, it is proper to calibrate the detector by the energy peak itself and results of the simulation. New energy spectrum applied these is shown in Fig.8.2

With regard to the later, we have considered that it was caused by the simultaneous Compton scatterings, that is, the several scattered photons simultaneously came into the detector and lost energy in the detector. We call these events as a double Compton scattering and a triple Compton scattering and so on. Considering these events, we have to simulate the response of the detector assuming that these events are generated according to Poisson distribution as

$$p(x) = \frac{m^x}{x!}\exp(-m), \tag{8.1}$$

where p is a probability, x is a number of simultaneous Compton scatterings and m is an average

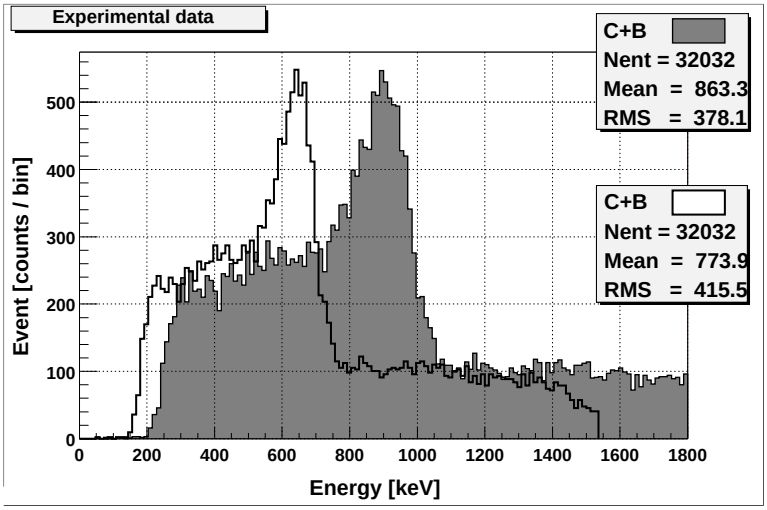

Fig.8.1: Energy spectra which the conditions of the calibrations are different each other. C and B represent numbers of Compton scattered photons and background respectively. The gray spectrum and the white one were calibrated with the electron beam off and on, respectively.

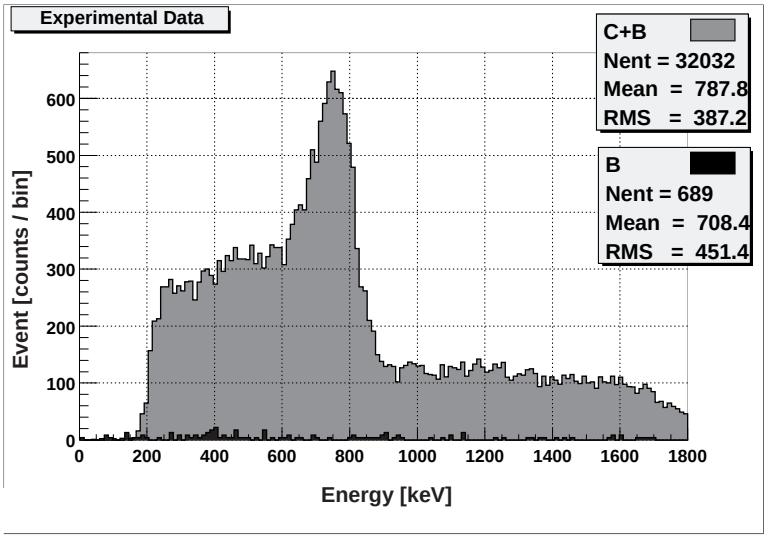

Fig.8.2 : Revised experimental energy spectra.

number of scattered photons which interact in the detector per a laser pulse, above 0.224, respectively. When m = 0.224, p(0) = 0.80, p(1) = 0.18 and p(2) = 0.02. The result of the simulation with these probability and experimental parameters is shown in Fig.8.3. In this figure, the numbers of the events over the peak and at 600keV are so few as compared with the experimental spectrum. The former implies that there was an unknown background when the laser beam irradiated the electron beam, and that experimental spectrum had more double Compton scatterings. The later implies that the resolution of the detector was worse than the known one, the aperture in front of the detector was actually opener than the measured one or both of them. We simulated the spectra about these. The results are shown in Fig.8.4, 8.5, 8.6 and 8.7. The parameters of these simulations are shown in Table.8.1. *m* is the average number of scattered photons, *a* is the aperture in front of the detector and r is the resolution of the detector. Unit of *a* is mm. "*r : nor.*" represents the resolution obtained in Fig.7.2. For example, "*r : 1.5*" represents that the resolution is one and a half times as the normal one. In Fig.8.7, the spectrum is similar to the experimental one except the shape of the peak and the number of the events over 1.6MeV. However, the parameter *m* used in the simulation 5 is impossible value in terms of this experiment. In these meanings, we suggest that there was the unknown background when the laser pulse irradiated the electron beam.

We also tried to align the optics for the laser multi pass system as shown in Section 3.6. We could align the optics so that there was the laser ablation inside of REFER which was caused by the reflections of the laser pulses on the surface of the glass windows for injecting the laser pulse as shown in Fig.8.8. This laser ablation resulted from the slope of these glass windows to the laser injecting and the recycling system. Finally, the experiment using this system was interrupted by it. We have to work out countermeasures about it.

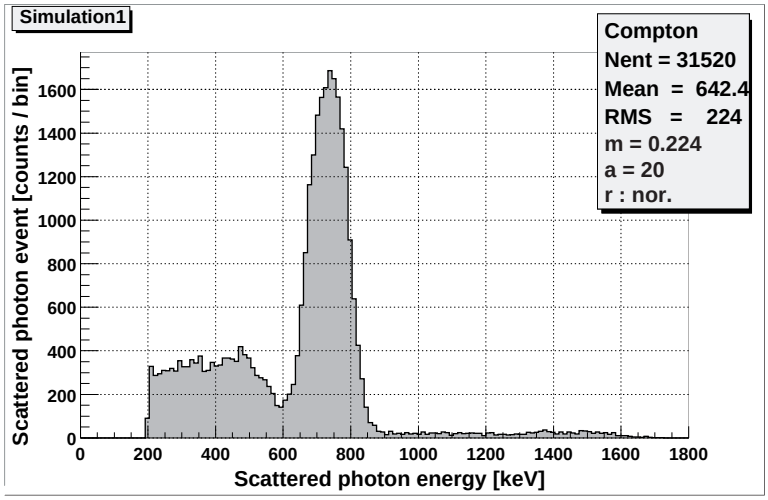

Fig.8.3: Simulated spectrum with experimental parameters. *m* is the average number of scattered photons, *a* is the aperture in front of the detector and r is the resolution of the detector. Unit of *a* is mm. "*r : nor.*" represents the resolution obtained in Fig.7.2. These symbols are common even in the below figures.

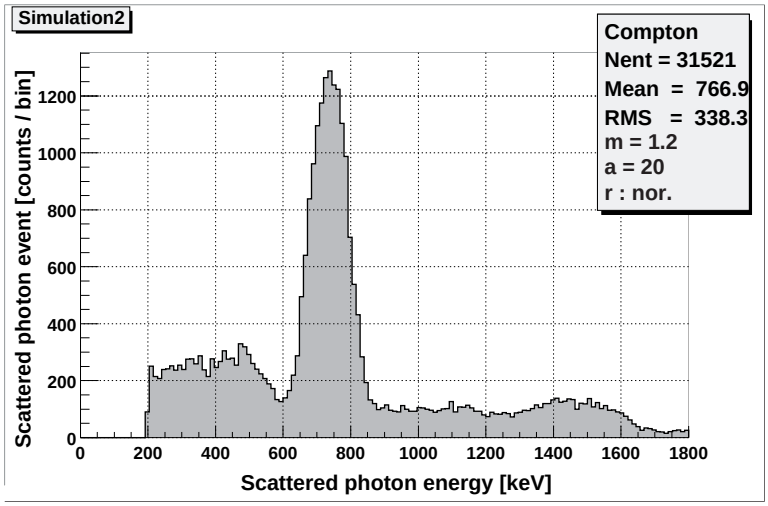

Fig.8.4: Simulated spectrum no.2.

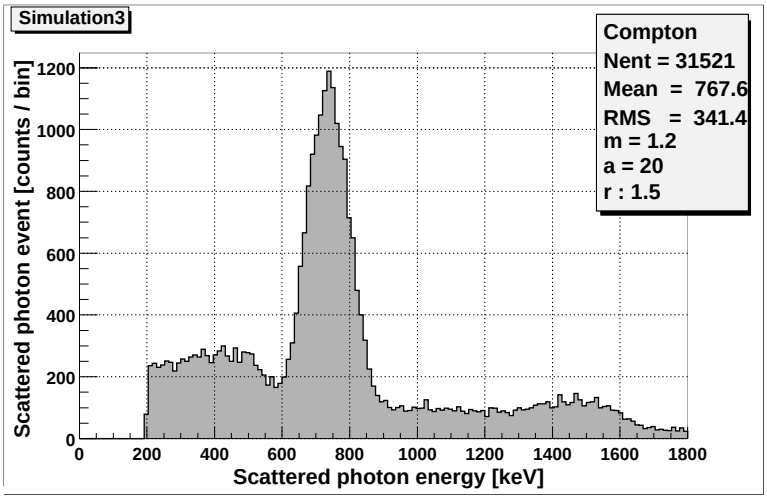

Fig.8.5 : Simulated spectrum no.3. "*r : 1.5*" represents that the resolution is one and a half times as the normal one. This representation are common in the below figures.

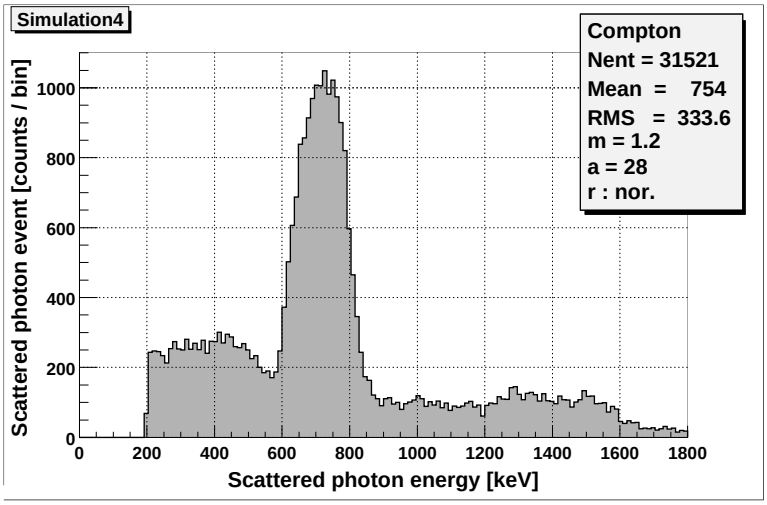

Fig.8.6: Simulated spectrum no.4.

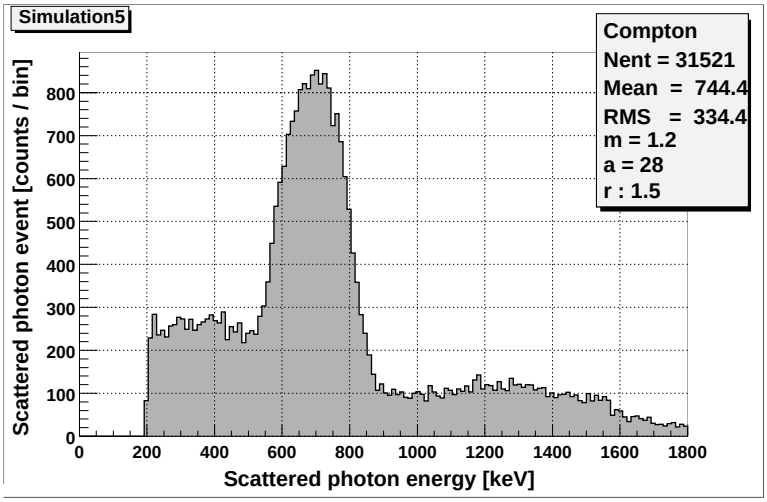

Fig.8.7: Simulated spectrum no.5.

Table.8.1: List of parameters in Simulations

	m	***a***	***R***
Fig.8.3	0.224	20	Normal
Fig.8.4	1.2	20	Normal
Fig.8.5	1.2	20	×1.5
Fig.8.6	1.2	28	Normal
Fig.8.7	1.2	28	×1.5

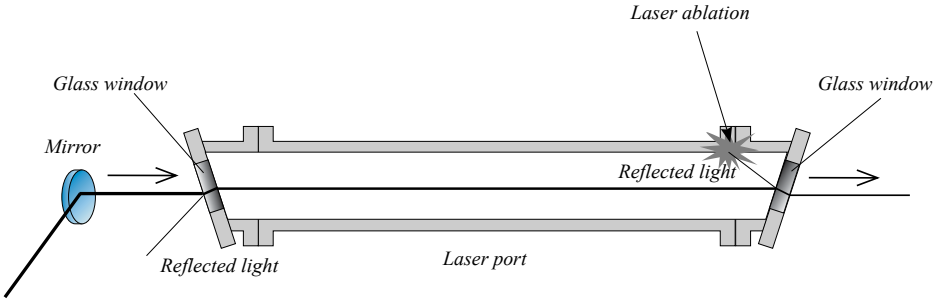

Fig.8.8: Laser ablation inside REFER. If we use the laser multi pass system, more laser ablation will happen.

9 Conclusion

We performed to Laser Compton scattering experiment, collisions between moving electron beams and laser beams, to generate X-ray at REFER in Hi-VBL. REFER and the laser system provide 150MeV electron beams and about 2eV laser beams.

As a result, we obtained the energy spectrum of scattered photons which had the energy peak at about 800keV, and this is consistent with the theory. The number of background, when the laser beam didn't irradiate the electron beam, was also so lower than Compton scattered photons. Therefore, X-ray generation by Laser Compton scattering was successful and we could construct the system to perform X-ray generation by this method. However, there were the considerable events over the energy peak, which is inconsistent with the kinematics of Laser Compton scattering. In order to verify these unknown events, we simulated the energy spectrum of scattered photons by Geant4. We simulated it by considering the existence of the simultaneous Compton scatterings, that is, the several scattered photons simultaneously came into the detector and lost energy in the detector. The simulated spectrum of scattered photons with just the experimental parameters was different from the experimental one with regard to the number of the events over the peak, but we obtained the similar spectrum as the experimental one changing the parameters consequently. However one of these parameters was realistically impossible value. It has been suggested that there was probably the unknown background when the laser pulse irradiated the electron beam.

We tried to construct the laser multi pass system. It is expected that the number of the scattered photons become 2~3 times as comparison with our usual single pass system. However, the laser ablation happened inside REFER so that we had to interrupt the experiment using this system. We have to work out countermeasures about it in future.

Acknowledgments

I would like to acknowledge many people’s help to the advance in Laser Compton scattering experiment. I am especially grateful to Dr. Tohru Takahashi for his much precise and effective advice to perform my study anytime. I am really thankful to Prof. Ichita Endo, Dr. Masataka Iinuma and Dr. Koji Matsukado for their valuable discussion and powerful support to progress my study. I want to express my gratitude for Mr. Kentaro Nakamura to join our experiments and work together for three years. I represent my thanks to Dr. Tomomi Ohgaki for the aggressive ideas, Ms. Yoshiko Okazaki for the intelligible lecture about Geant3, Mr. Takehiro Ohnishi for the point-blank leading about the vacuum system, Mr. Kiminori Goto for good supply of electron beam to REFER and Mr. Daisuke Iseki, Mr. Shinji Ikuta and Mr. Kazuaki Kozawa for their unexpected strong cooperation.

In the end of this thesis, I wish to thank my parents, Kazuo and Ikuko Kimura and my brothers Yusuke and Hiroyuki for their invisible ones.

Reference

[1] T. Ohgaki, “Higgs Boson Study at Photon-Photon Colliders”, Hiroshima University, 1998

[2] Berestetskii, V. B., Lifshits, E. M., Pitaevskii, Lev Petrovich, “Relativistic quantum theory”, Tokyo Library, Inc., 1969 [in Japanese]

[3] H. Ozaki, Graduate Thesis, Hiroshima University, 2000 [in Japanese]

[4] Y. Itogawa, Graduate Thesis, Hiroshima University, 1998 [in Japanese]

[5] K. Matsukado, “Experimental study for nonlinear Compton scattering”, Hiroshima University, 2000

[6] Y. Matsui, ISBN 4-7665-0601-4, Keigaku publishing, Inc., 1988[in Japanese]